

# PCCP

Accepted Manuscript



This is an *Accepted Manuscript*, which has been through the Royal Society of Chemistry peer review process and has been accepted for publication.

*Accepted Manuscripts* are published online shortly after acceptance, before technical editing, formatting and proof reading. Using this free service, authors can make their results available to the community, in citable form, before we publish the edited article. We will replace this *Accepted Manuscript* with the edited and formatted *Advance Article* as soon as it is available.

You can find more information about *Accepted Manuscripts* in the [Information for Authors](#).

Please note that technical editing may introduce minor changes to the text and/or graphics, which may alter content. The journal's standard [Terms & Conditions](#) and the [Ethical guidelines](#) still apply. In no event shall the Royal Society of Chemistry be held responsible for any errors or omissions in this *Accepted Manuscript* or any consequences arising from the use of any information it contains.

**Transformation of Photophysical Properties**  
**From Solution to Solid State in**  
**Alkoxy-Cyano-Diphenylacetylene Molecules**

*Venugopal Karunakaran<sup>a,b\*</sup>, Deepak D. Prabhu<sup>a</sup>, Suresh Das<sup>a,c\*</sup>, Sunil  
Varughese<sup>d</sup>*

<sup>a</sup>Photosciences and Photonics Section, Chemical Sciences and Technology Division, CSIR-National Institute for Interdisciplinary Science and Technology, Thiruvananthapuram 695 019, Kerala, India. <sup>b</sup>Academy of Scientific and Innovative Research (AcSIR), New Delhi 110 001, India. <sup>c</sup>Jawaharlal Nehru Centre for Advanced Scientific Research, Bangalore 560 064, India, <sup>d</sup>Materials Sciences and Technology Division, CSIR-National Institute for Interdisciplinary Science and Technology, Thiruvananthapuram 695 019, Kerala

## Abstract

Detailed photophysical properties of cyano and mono (MA)/ bis alkoxy(DA) substituted diphenylacetylene moiety with different alkyl chain lengths (methyl (1), octyl (8) and dodecyl (12)) were investigated in solution and solid state in an effort to determine the role of self-aggregation on these properties. The solvated molecules showed minimal bathochromic shift with increase of solvent polarity in their absorption spectra, whereas significant shift was observed in the emission spectra. This could be attributed to relatively low change in dipole moment between ground and Franck Condon excited state and luminescence arising from the intramolecular charge transfer state with dipole moment significantly higher than the ground state. In solid state the emission quantum yields of these materials were significantly higher than in solution. For DA1, polymorphic materials with distinct photophysical properties were obtained. The DA1 materials obtained by fast precipitation (DA1) showed broad fluorescence with peaks at 398, 467 and 535 nm by exciting at different wavelength. Detailed analysis of absorption, emission and excitation spectra and lifetime experiments indicated that these peaks could be attributed to the monomer, J- and H-type aggregates respectively. Whereas the crystals obtained by slow crystallization (DA1C) showed only one emission peak around 396 nm attributed to the monomer. This is supported by the single crystal X-ray structure which consists of monomer molecule having minimal interaction with nearest neighbour molecules.

**Key words:** Solid state emission, Polymorphism, Aggregation, Time resolved emission, Charge transfer state.

## 1. Introduction

Intensive research has been focused on understanding the electronic and optical properties of electron donor (D) and acceptor (A) substituted  $\pi$ -conjugated materials in view of their potential applications in a wide range of areas including energy-efficient lighting<sup>1-7</sup>, microcavity resonators<sup>8,9</sup> and field effect transistors<sup>10-14</sup>, biosensors and bio-imaging agents<sup>15, 16</sup>. The optical properties of such molecules can be tuned by varying the nature of the donor and acceptor groups as well as the length and nature of the conjugating moiety<sup>17, 18</sup>. The optical properties of these materials in the solid and thin film states, conventionally used in most applications, can change dramatically in an unpredictable manner when compared to that of the free molecules in solution. For instance aromatic compounds such as pyrene, fluorescein, naphthalene, anthracene, phenanthracene, triphenylamines, and carbazole<sup>19-21</sup> are strongly fluorescent in solution but non-fluorescent in the solid state. Conversely there are a few compounds which are non-fluorescent in solution and highly fluorescent in the solid state<sup>22, 23</sup>. This change is brought about by factors including rigidization of the molecule in the solid state and various intermolecular interactions between neighbouring molecules<sup>17, 24</sup>. Such intermolecular interactions between neighbouring molecules can lead to the formation of two types of aggregates, namely J<sup>25-27</sup>-aggregates which have characteristic features of narrow red shifted absorption spectra and strong emission with high radiative constant, compared to H<sup>28, 29</sup>-aggregates which possess broadened blue shifted spectra and are practically non-luminescent due to low radiative constants. Even though a number of studies have been carried out to elucidate the nature and effect of such interactions, sufficient understanding is not yet available to make it possible to tailor the optical properties of materials in the solid state. For example a number of recent studies have shown that for certain molecules form H-aggregates which are highly emissive. Examples include

disubstituted polyacetylenes<sup>30</sup>, mero<sup>31</sup>- and hemicyanine<sup>32</sup> based chromophores, perylene bisimides<sup>33, 34</sup>, and polyquinolines<sup>35</sup>.

Though the photophysical properties of phenylethynyl (Ph-C≡C)-linked  $\pi$ -conjugated systems<sup>36, 37</sup>, especially central core of diphenylacetylene (DPA) have been widely investigated in solutions<sup>38-41</sup>, the solid state photophysical properties of DPA derivatives have not been explored in detail<sup>42, 43</sup>. Here we report a detailed study of two series of mono- and di alkoxy substituted diphenylacetylene derivatives (Figure 1), containing cyano as the acceptor group, which show significant differences in their photophysical properties in solution and in the solid state and elucidate the nature of neighbouring molecule interactions which lead to these differences. It was found that these derivatives exhibited significantly higher fluorescence quantum yields in the solid state compared to the solution. Hence these materials could be applied for organic optoelectronic devices.

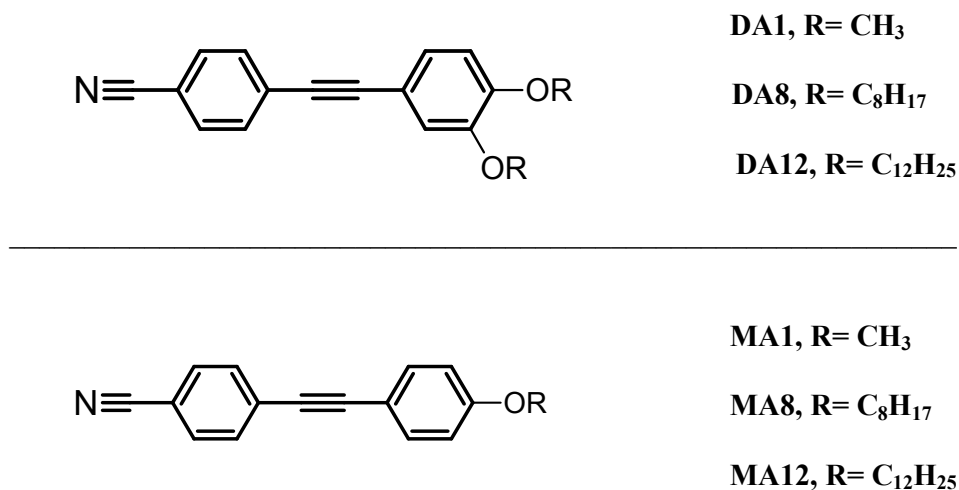


**Figure 1** Chemical structures of alkoxy-cyano diphenylacetylene derivatives.

## 2. Experimental Section

### 2.1 General remarks

The reagents and materials used for synthesis were purchased from Sigma-Aldrich, Merck and Spectrochem Chemical suppliers. Dry solvents were used wherever necessary and prepared by following the reported procedures<sup>44</sup>. <sup>1</sup>H-NMR spectra were recorded using DPX 500 MHz spectrometer using tetra-methylsilane (TMS) as the internal standard and deuterated solvents were used for the measurements.

### 2.2 Synthesis of mono and bis alkoxy substituted derivatives

The synthetic routes, molecular structure of the intermediates and final compounds 4-[(3,4-bisalkoxyphenyl)ethynyl]benzotrile ( (DA1), (DA8) and (DA12)) and 4-[(4- alkoxy phenyl) ethynyl]benzotrile ( (MA1), (MA8) and (MA12)), used in this study are shown in scheme S1 and S2 respectively in the Supporting Information. The experimental details and structural characterization by <sup>1</sup>H NMR, <sup>13</sup>C NMR, and mass spectral data are provided in the Supporting Information.

The purest forms of solid materials (powder) were prepared by fast precipitation by adding excess of *n*-hexane to saturated THF solutions. Whereas the single crystals were obtained by slow evaporations of small amount of the compounds dissolved in THF.

### 2.3 Instrumentation

Absorption spectra were recorded using a Shimadzu UV-2600 UV-Visible spectrophotometer. The optical diffuse reflectance spectra were measured for solid samples with aforementioned spectrometer equipped with an integrating sphere. BaSO<sub>4</sub> was used as the reference material, and the solid samples were ground well before the measurement. The absorption ( $\alpha/S$ ) data were calculated from the reflectance spectra using the Kubelka–Munk function:  $\alpha/S = (1-R)^2/2R$ , in which R is the reflectance at a given wavelength,  $\alpha$  is the

absorption coefficient, and  $S$  is the scattering coefficient (practically wavelength independent when the particle size is larger than  $5 \mu\text{m}$ ). Steady-state fluorescence experiments were performed with a FluoroLog-322 (Horiba) which was equipped with a 450W Xe arc lamp by using optically dilute solutions. The fluorescence quantum yields in various solvents were determined with the relative method employing an optically matched solution of quinine sulphate in 0.1N sulphuric acid as the reference ( $\Phi_R = 0.54$ ). The following equation was used for calculating quantum yield,

$$\Phi_S = \frac{\text{Abs}_R}{\text{Abs}_S} \times \frac{\text{Area}_S}{\text{Area}_R} \times \frac{n_S^2}{n_R^2} \times \Phi_R \quad (1)$$

Where the subscript R and S refers to the reference and samples respectively. Abs, Area and  $n$  are the absorbance at the excitation wavelength, area under the fluorescence spectrum and refractive index of the solvent respectively. Solid state photoluminescence spectra were also recorded using the front face mode with the same Fluorolog spectrofluorimeter. The solid-state absolute fluorescence quantum yields were determined using an integrating sphere following a reported procedure<sup>45</sup>. The solid-state fluorescence quantum yield of tris-8-hydroxyquinolino aluminum (Alq3) measured as a standard was  $19 \pm 2 \%$  consistent with previously reported values<sup>46</sup>.

Time-resolved fluorescence spectra and lifetime experiments were performed by using an IBH picosecond single photon counting system employing the 277, 335 and 375 nm nano LED as excitation sources and a Hamamatsu C4878-02 microchannel plate (MCP) detector. Decay in the fluorescence intensity ( $I$ ) with time ( $t$ ) was fitted either by a double/triple-exponential function:

$$I = A_1 e^{-t/\tau_1} + A_2 e^{-t/\tau_2} \quad (2)$$

$$I = A_1 e^{-t/\tau_1} + A_2 e^{-t/\tau_2} + A_3 e^{-t/\tau_3} \quad (3)$$

Where  $\tau_1$ ,  $\tau_2$ , and  $\tau_3$  are the lifetimes of different species, and  $A_1$ ,  $A_2$ , and  $A_3$  are their respective amplitudes. The weighted mean lifetime ( $\langle\tau\rangle$ ) was calculated according to eqn.4:

$$\langle\tau\rangle = \sum \tau_i A_i \quad (4)$$

The quality of the fits was checked by examining the residual distribution and the  $\chi^2$  value. The solid state samples were recorded with front face mode. All the experiments were conducted at room temperature.

Single crystal suitable for X-ray diffraction studies was carefully chosen after they were viewed through a microscope supported by a rotating polarizing stage and a CCD camera. The diffraction data of single crystals were collected on a Rigaku Saturn 724+ diffractometer using graphite monochromated Mo- $K_\alpha$  radiation ( $\lambda = 0.71073\text{\AA}$ ). In these cases, data were processed with the Rigaku Crystal Clear software<sup>47, 48</sup>. The structure solution was carried out by direct methods, and the refinements were performed by full-matrix least-squares on  $F^2$  using the SHELXTL<sup>49</sup> suite of programs. All calculations of intermolecular interactions were done with the HBOND NORM option of PLATON<sup>50</sup>.

#### 2.4 Electronic structure calculation

The structures of DA and MA derivatives were optimized with density-functional theory (DFT) method implemented in the Gaussian 09 software package<sup>51</sup>. The ground state geometry was optimized at the CAM B3LYP/6-31G(d) level of theory with vibrational frequencies calculated at the same level. The vertical excitation energy of optimized structure was calculated with time-dependent density function theory (TDDFT) method at the CAM B3LYP/6-31G(d) level of theory.

### 3. Results and Discussion

#### 3.1 Photophysical Studies in Solution State

The absorption and emission spectra of **DA** and **MA** derivatives were measured in solvents of varying polarity. Figure 2 shows the absorption and emission spectra of the **DA** and **MA** derivatives in acetonitrile. It was observed that the absorption spectra of the two series of compounds were nearly the same, with the emission spectra of the **DA** series being red-shifted when compared to that of the **MA** derivatives. There was little or no effect in the absorption and emission spectra on the change in alkyl chain length within the **DA** and **MA** series.

Figure 3 shows the absorption and emission spectra of bismethoxy cyano derivative (**DA1**) in hexane, chloroform and acetonitrile. The absorption spectrum of **DA1** in hexane exhibited a vibrational structure whereas in the polar solvents such as acetonitrile, the absorption spectrum was broad and structureless. There was however no significant change in the absorption maxima with increase in solvent polarity. This is indicative of the dipole moments of their ground and excited state being very similar, reflecting insignificant amount of charge transfer character in the Franck Condon (FC) excited state. The fluorescence spectra however exhibited significant bathochromic shift with increase of solvent polarity. The broadening of the emission spectra with increase of solvent polarity could be due to the change of conformation. For example the emission maxima of **DA1** in hexane appeared at 346 nm, whereas in polar dimethyl sulfoxide, it was highly red shifted to 462 nm. This reflects that direct excitation of these molecules leads to a weakly emitting locally excited state (FC) possessing nearly the same dipole moments as the ground state, which transforms in to a more polar emissive state via an intramolecular charge transfer (ICT) process.

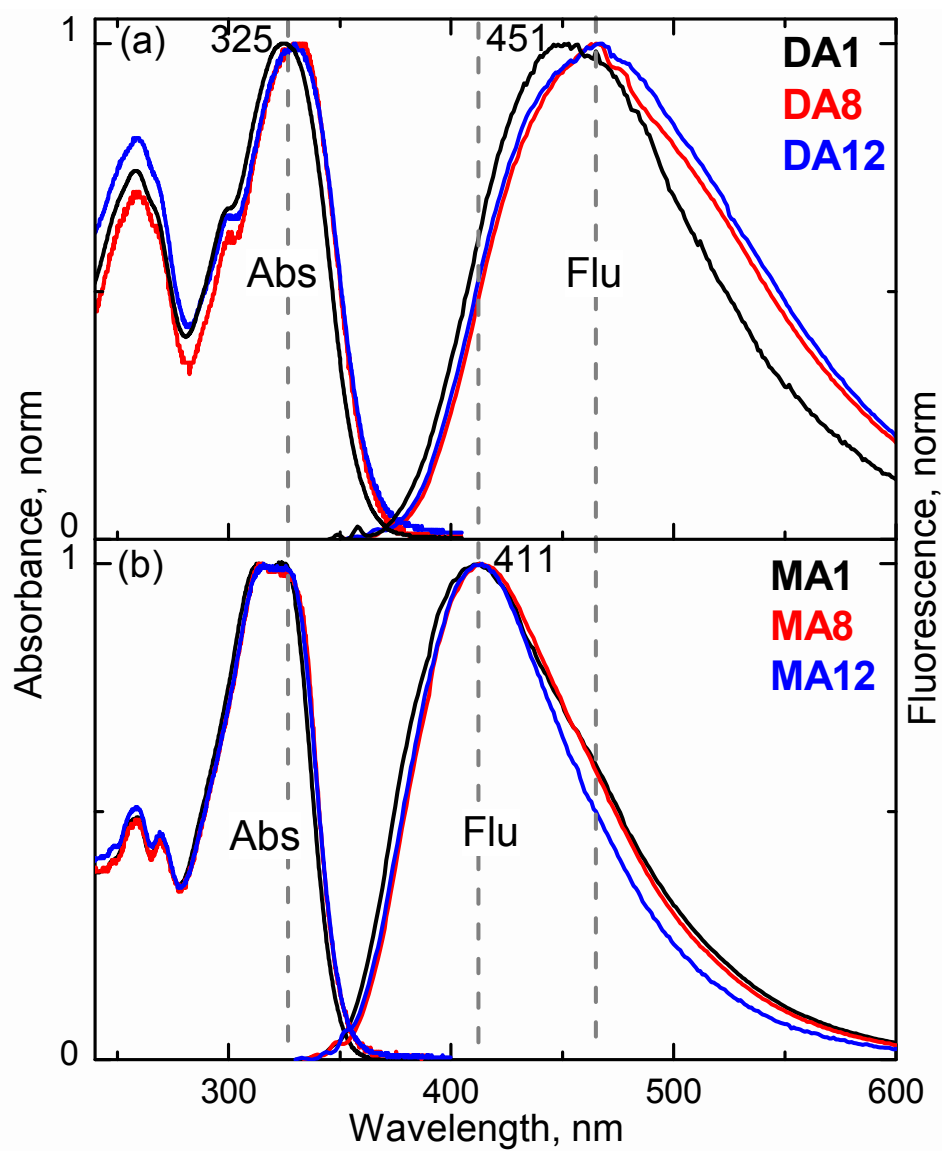


**Figure 2** The absorption and fluorescence spectra of **DA** (a) and **MA** (b) derivatives in acetonitrile are shown for comparison. The methyl(1), octyl(8) and dodecyl(12) substituents are shown in black, red and blue colours respectively.

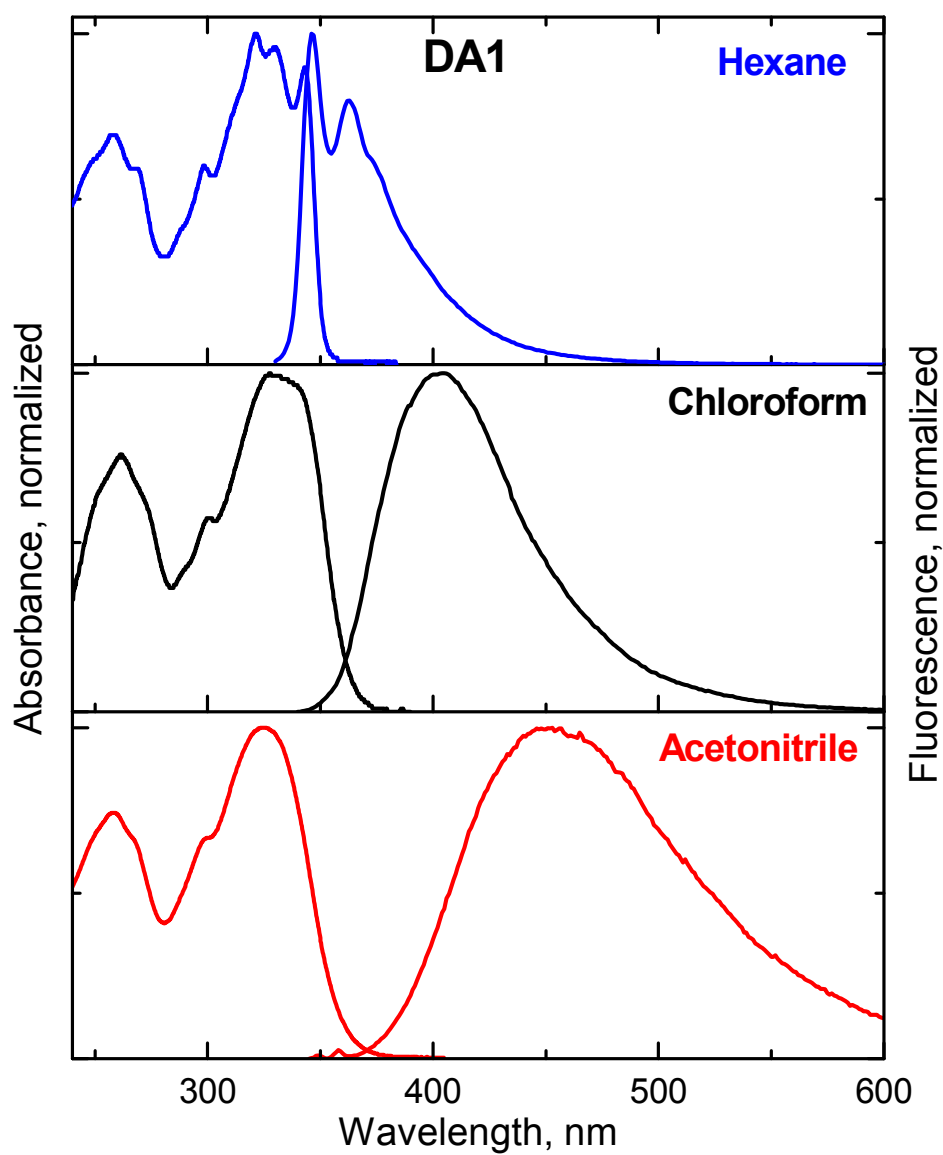


**Figure 3** Steady state absorption and fluorescence spectra of **DA1** in *n*-hexane (blue), chloroform (black) and acetonitrile (red) at room temperature.

This was evidenced by the existence of separated LE and ICT states which were clearly seen in the emission spectra of **DA1** in acetonitrile (Figure 3 and S1 in the Supporting Information). Here the emission arising from the LE state, vibronic in nature, was feebly seen in the blue side of the intense ICT band. Similar kinds of observations were already reported in the literatures<sup>52-55</sup>.

The effect of solvent polarity on the absorption and emission spectra of **MA1** was very similar to that observed for **DA1** (Figure S2 supporting information)<sup>41</sup>. The fluorescence lifetimes of the derivatives in different solvents were measured by exciting at 335 nm using nano second LED sources. The representative fluorescence kinetic traces for **DA1**(a) and **MA1**(b) in hexane, chloroform and acetonitrile are shown in Supporting Information as Figure S3. The fluorescence quantum yields of the derivatives in different solvents were calculated and found to be around  $0.20 \pm 0.05$ . The radiative and nonradiative rate constants were also calculated from fluorescence quantum yields ( $\Phi$ ) and average lifetimes ( $\tau_f$ ) using the following equation and provided in Table 1

$$k_r = \frac{\Phi}{\langle \tau_f \rangle} \quad \text{and} \quad k_{nr} = \frac{1}{\langle \tau_f \rangle} - k_r \quad (5)$$

where  $k_r$  and  $k_{nr}$  represent the radiative and non-radiative rate constants, respectively. The spectroscopic and photophysical properties of the derivatives are summarized in Table 1 and 2, and ST1 to ST4 in the Supporting Information. Here it is to be noted that the aggregation of these compounds were not observed with increase of concentration or in the mixture of solvents even with water (Figure S4 in Supporting Information).

In general, the absorption and fluorescence spectra of all the compounds showed vibronic structure in non-polar solvents, whereas they were broadened in the more polar solvents. Over all with the addition of another alkoxy group resulted in a larger red shifted fluorescence, increase in fluorescence lifetimes and quantum yields. This can be attributed to

the presence of the additional alkoxy group causing an enhancement in the electron-donating capabilities of the phenyl moiety leading to increased formation of the fluorescent ICT state at the cost of the weakly fluorescent LE state. This is supported by higher negative electrostatic potential on the dialkoxy groups, seen in the electrostatic potential isosurface of **DA1** obtained by theoretical calculations performed using density functional theory (DFT) with the CAM B3LYP hybrid functional and 6-31G(d) basis set (Figure 4).

The theoretically optimized results of energy, absorption maxima with oscillator strength and ground state dipole moments are provided in Table 3. The  $S_0 \rightarrow S_1$  transition is from the highest occupied molecular orbital (HOMO) to the lowest unoccupied molecular orbital (LUMO) for all the derivatives. It is interesting to note that the HOMO orbitals were concentrated on the methoxy substituted phenyl ring and with lesser electronic distribution on cyano substituted phenyl ring. Whereas in LUMO or LUMO+1, the electronic contribution is highly concentrated on the cyano substituted phenyl ring for both the derivatives. The simulated absorption maxima for the compounds is in agreement with the experimental value within acceptable limits. In order to understand the electrostatic potential differences between **DA1** and **MA1**, molecular electrostatic potential energy (MESP) surface for both the **DA1** and **MA1** was generated having range from  $\pm 35.9 \text{ kcal mol}^{-1}$  (Figure 4B). Over all the total molecular electrostatic potential pattern is relatively similar except that **DA1** has more negative electrostatic potential at around the alkoxy substituents ( $28.9 \text{ kcal mol}^{-1}$ ) compared to that of **MA1** ( $12.5 \text{ kcal mol}^{-1}$ ) and it needs further investigation.

In order to estimate the dipole moment change between the ground and excited states, the solvatochromic shifts of these compounds were analysed with Lippert–Mataga function which dealt for dipolar interaction. It is to be noted that as the excitation spectra of **DA1** in

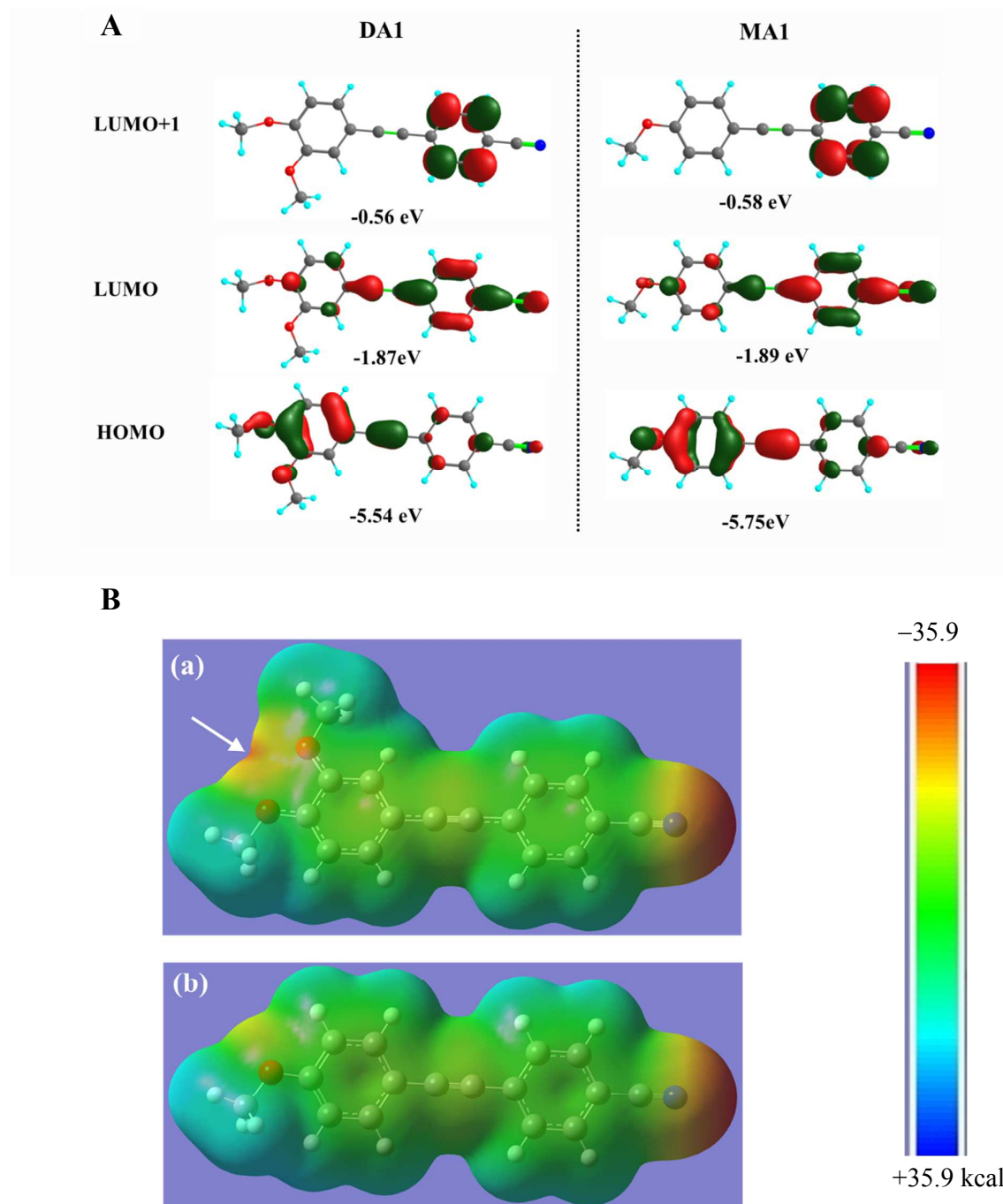


**Figure 4** **A** CAM B3LYP/6-31G(d) derived contour surface diagrams of molecular orbitals involved in the dominant low-energy electronic transitions for **DA1**(left) and **MA1**(right) with their corresponding energy levels. **B**. The electrostatic potential mapped on electron density surface value of 0.0004 ranging from  $\pm 35.9$  kcal mol<sup>-1</sup> for **DA1**(a) and **MA1**(b). The most positive and negative electrostatic potential regions are depicted in blue and red. The green represents a potential halfway between the two extremes. The negative electrostatic potential near alkoxy group(s) is 28.9 and 12.5 kcalmol<sup>-1</sup> for **DA1** and **MA1** respectively.

polar solvents resembled to its absorption spectra (Figure S1), the origin of ICT state could be from the local excited state<sup>56</sup>. Hence Lippert–Mataga function was used to tentatively find the excited state dipole moments. The Stokes shift were calculated from the absorption and emission maxima and listed in the Table 1 and 2, and ST1 to ST4 in the Supporting Information. The excited state dipole moments were obtained by fitting the dynamic Stokes shift to the Lippert–Mataga<sup>57,58</sup> equation (6).

$$\nu_a - \nu_f = \frac{2(\mu_e - \mu_g)^2}{hca^3} \left[ \frac{\epsilon - 1}{2\epsilon - 1} - \frac{n^2 - 1}{2n^2 - 1} \right] \quad (6)$$

where  $a$ , the cavity radius was calculated using the equation (7)

$$a(\text{in } \text{Å}) = \sqrt[3]{[(3 \times 1.33 \times v_w)/4\pi]} \quad (7)$$

$v_w$ , volume of van der Waals surface of the molecules obtained by using Discovery Studio Visualizer v. 2.0 (Accelrys software Inc). The Lippert–Mataga plot of Stokes shift vs. solvent parameter is shown in Figure 5 for the compounds **DA1** and **MA1**. (Here 1,4 dioxane and propanol have not been included in the plot as they are deviating from the linear fit. This could be due to the anomaly behaviour of dioxane<sup>59</sup> and formation of hydrogen bond with compounds by propanol). It is important to note that there is a linear correlation between the polarizability and Stokes shift of **DA1** and **MA1**. The intensification of the CT character with increasing number of electron donating groups in **DA1** is inferred from the increase of slope for **DA1** compared to **MA1**. The values  $(\mu_e - \mu_g)$ , obtained for these selected compounds are positive, which means that the excited state is more polar than the ground state. The estimated change of dipole moments between ground and excited state (7.02 D (**DA1**) and 5.92 D (**MA1**)) from the Lippert–Mataga plot reflect that CT character is more pronounced in **DA1** derivative. Overall from the ground state dipole moment ( $\mu_g$ ) and change in dipole moment  $(\mu_e - \mu_g)$ , excited state dipole moment ( $\mu_e$ ) determined to be 13.74 D and 12.79 D for

**DA1** and **MA1** respectively reflecting the presence of highly polar ICT state in these compounds.

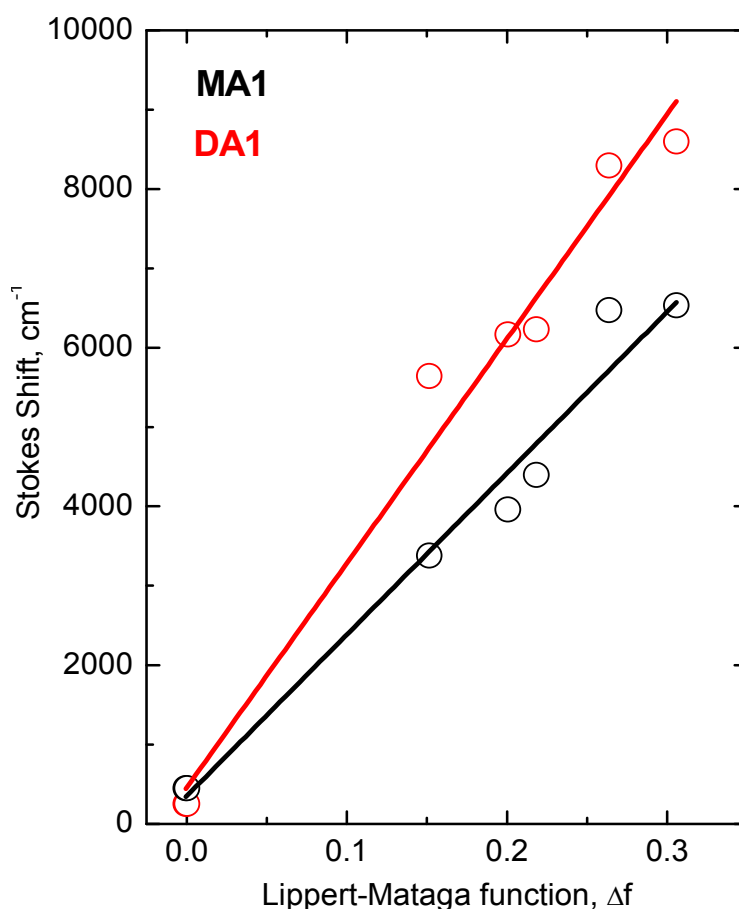


**Figure 5** Plot of Stokes shift ( $\Delta\nu$ ) versus the solvent polarity function of Lippert–Mataga function ( $\Delta f$ ) for **DA1** (red) and **MA1** (black) in various solvents. Solid lines are the fitted ones.

### 3.2 Photophysical Studies in Solid State

The absorption spectra of the **DA** and **MA** derivatives measured in the solid state are shown in Figure 6. The normalized absorption spectra of **DA** derivatives (Figure 6a) showed maxima around 310 and 370 nm. The ratio of the absorbance between 310 and 370 nm varied with length of the alkyl substituent. The relative increase in absorbance at around 370 nm was in the order of **DA8** < **DA12** < **DA1** reflecting more contribution from the J- type aggregates in **DA1** and consistent with the fluorescence quantum yields (*vide infra*).

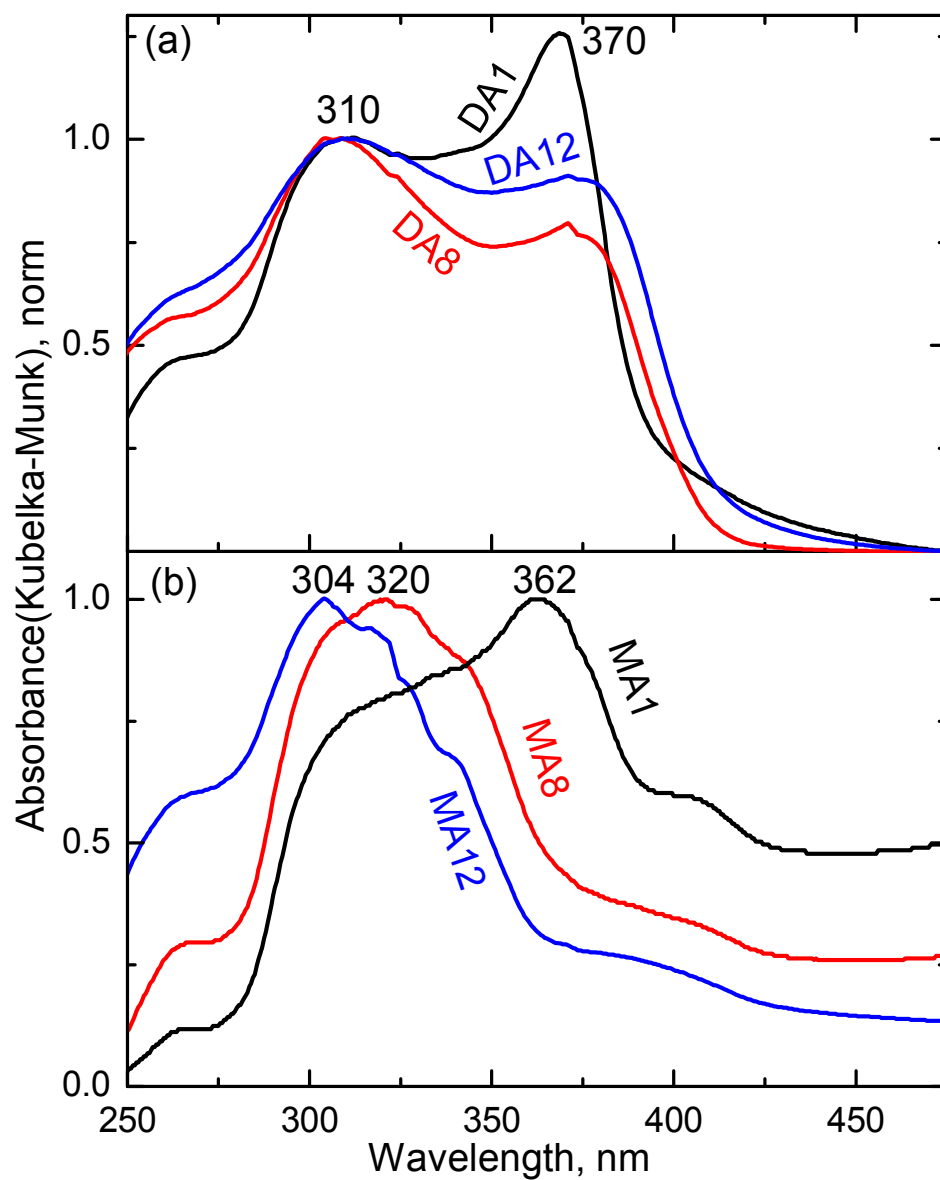


**Figure 6** Normalized absorption spectra of **DA**(a) and **MA**(b) derivatives in solid state. Methyl(**1**), Octyl(**8**) and dodecyl(**12**) derivatives are shown in black, red and blue colour respectively.

The emission spectra of **DA** derivatives obtained by exciting at different wavelength starting from 290 to 450 nm covering entire absorption spectra are shown in Figure 7. In figure 7a, it is interesting to note that excitation at 290 nm, which is in the blue side of the absorption maxima of **DA1** showed two emission maxima, one at ~398 nm and another broad band at ~543 nm. On gradually increasing the excitation wavelength to 360 nm, the emission intensity around 543 nm decreases gradually but the intensity of emission maximum around 398 nm does not change significantly. Further increase in the excitation wavelength leads to a decrease in the fluorescence intensity around 398 nm, and this is accompanied by the formation of a new emission band with a maximum centered at 467 nm. The significant change in the emission spectra with change in excitation wavelength observed for **DA1** was not seen for **DA8** (Figure 7b). Whereas for **DA12** (Figure 7c), it showed two different emission maxima at 444 and 508 nm by exciting at 300 and 430 nm respectively. The change of emission spectra with different excitation wavelength for these materials could be due to variation in the molecular packing which controls their solid state fluorescence behaviour.

The normalized emission spectra for the three derivatives excited at different wavelengths are summarized in Supporting Information as Figure S5. The panel a of Figure S5 shows the normalized emission spectra of **DA1** obtained by exciting at 310 and 390 nm for comparison. The corresponding excitation spectra obtained by monitoring emission at 398, 467 and 543 nm are shown in the supporting information as Figure S6. The appearance of various emission maxima in **DA1** indicate the presence of different emitting species. The emission band centred at 398 nm can be attributed to monomer emission. While the highly red shifted emission centred at 543 nm can be attributed to excitation of H-aggregates which can lead to formation of excimers emitting in this region. It is noted that the emission peak at 543 nm could not be due to the intramolecular charge transfer or by the planarization as its

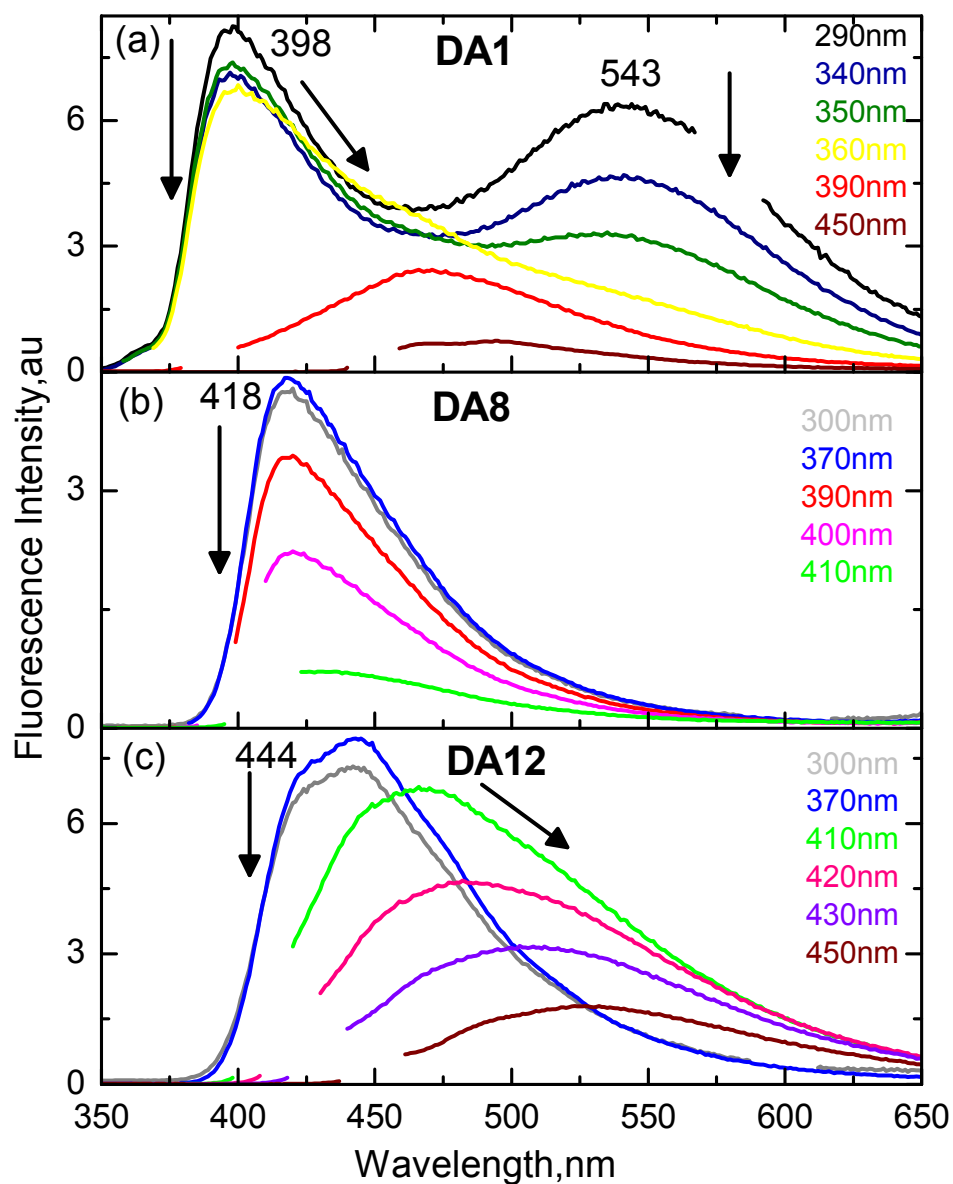


**Figure 7** Fluorescence spectra of DA derivatives of DA1(a), DA8(b) and DA12(c) in solid state obtained by exciting at different wavelength. The representative excitation wavelengths are shown in different colours. The spectral changes with increase of excitation wavelength are shown by the arrows.

intensity was strongly dependent on the excitation wavelength and the diluted materials by KBr resulted the conversion of the aggregated species observed in the bulk samples to that of monomer (Figure S7).

On increasing the excitation wavelength to 360 nm, the long wavelength emission band disappears leaving only the emission band centred at 398 nm attributable to emission from the excited monomer. Further increase in the excitation band leads to the appearance of a new emission band centred at 467 nm. Since this emission band appears on excitation on the red side of the monomer absorption band it can be attributed to arise from excitation of the J-type aggregates led to J-type excimer<sup>31, 34, 60</sup>. The appearance of such a blue shifted emission by the J-type aggregates compared to the H-type aggregates was reported in the literatures<sup>61</sup>. For **DA8** (Fig.7b) the emission spectra did not depend on the wavelength of excitation, with mainly the monomer emission being observed. In the case of **DA12** (Fig.7c), the broad peak at 444 nm could be due to a mixture of emission from the monomeric and aggregated forms. The peak centred at 508 nm which is observed on excitation at 430 nm can be attributed to excitation of the J-type aggregates. The mode of linking or driving force for the formation of J- and H- aggregates could depend on the relative positions of adjacent molecules and their dipole moments<sup>62-64</sup>.

The absorption spectra of the **MA** derivatives in the solid state were very broad (Figure 6b), **MA1** showed maximum around 362 nm with shoulders around 310 and 400 nm. With increase of alkyl chain length, absorption maximum was blue shifted indicating the formation of H-type aggregates<sup>54</sup>. The emission spectra were measured by exciting at wavelengths ranging from 300 to 450 nm. For **MA1** no significant change was observed in the emission spectrum with change in excitation wavelength (Figure 8a). Maximum intensity of emission was observed at 391 nm on excitation at 300 nm. For both **MA8** and **MA12** two kind of emission bands were observed depending upon wavelength of excitation.

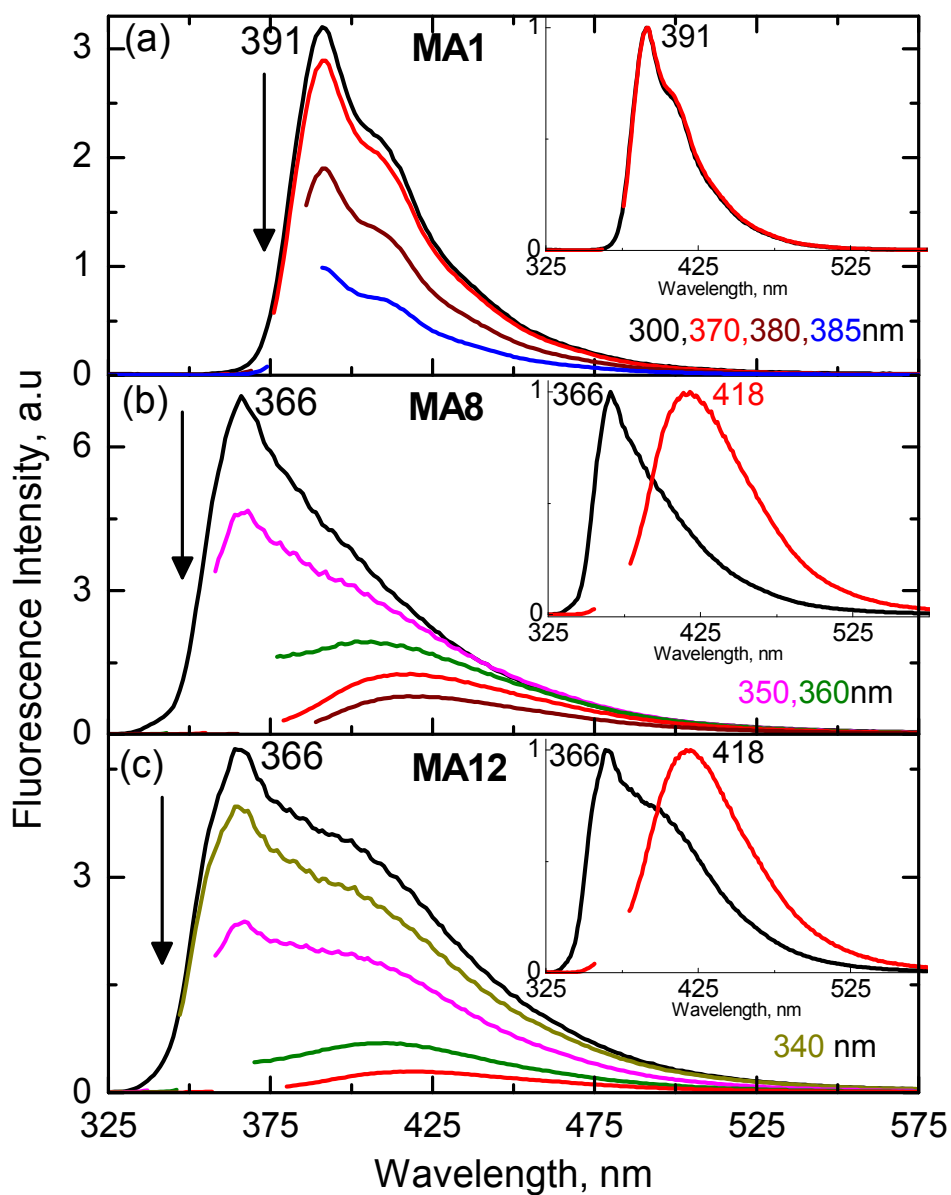


**Figure 8** Fluorescence spectra of MA derivatives of MA1 (a), MA8 (b) and MA12 (c) in solid state obtained by exciting at different wavelength. The inset shows normalized fluorescence spectra obtained by exciting at 310 and 370 nm for all the derivatives for comparison.

Excitation around 300 nm lead to an emission band centred at 366 nm whereas excitation at 370 nm led to emission band centred at 418 nm (Figure 8b and c).

Based on comparison with the **DA** derivatives, the short and long wavelength emission in **MA** derivatives can be attributed to the monomer and the J-type aggregates respectively. Solid state luminescence quantum yields were measured using an integrating sphere and Alq3 as a standard, by following reported procedures<sup>46</sup>, and the values are summarized in Table 4. **DA1** had the highest fluorescence quantum yield (0.8) among these derivatives. The difference of fluorescence quantum yields of these materials could be due to the formation of various amounts of monomer, J- and H-aggregates. The comparison of fluorescence quantum yields of both the **DA/MA** derivatives between the solid (~0.80/0.65) and solution state (~0.2 / 0.15) revealed the phenomenon of aggregation induced enhanced emission in the solid state<sup>22</sup>.

The fluorescence lifetime of all the materials in the solid form were measured by using nanosecond LED sources and the kinetics was fitted with either two or three exponentials. The fitted results for all the derivatives are also shown in Table 4. The representative fluorescent decay profiles of **DA1** and **MA1** materials obtained by excitation at 277 and 375 nm are shown in the Figure 9 and in Supporting Information as Figure S8 respectively. On excitation at 277 nm, the major components have fluorescence lifetimes of 0.93 and 1.3 ns probed at 398 and 543 nm respectively. The lifetime of ~0.93 ns could correspond to the monomeric emission, while the component with a lifetime of 1.3 ns obtained on excitation (277 nm) and probing at red side (543 nm) for **DA1** could be due to the exciplex/excimer formed on excitation of the H-type aggregates<sup>31, 34, 60</sup>. On excitation of **DA1** at 375 nm and probing at 467 nm a long lived component of 12.3 ns was obtained.

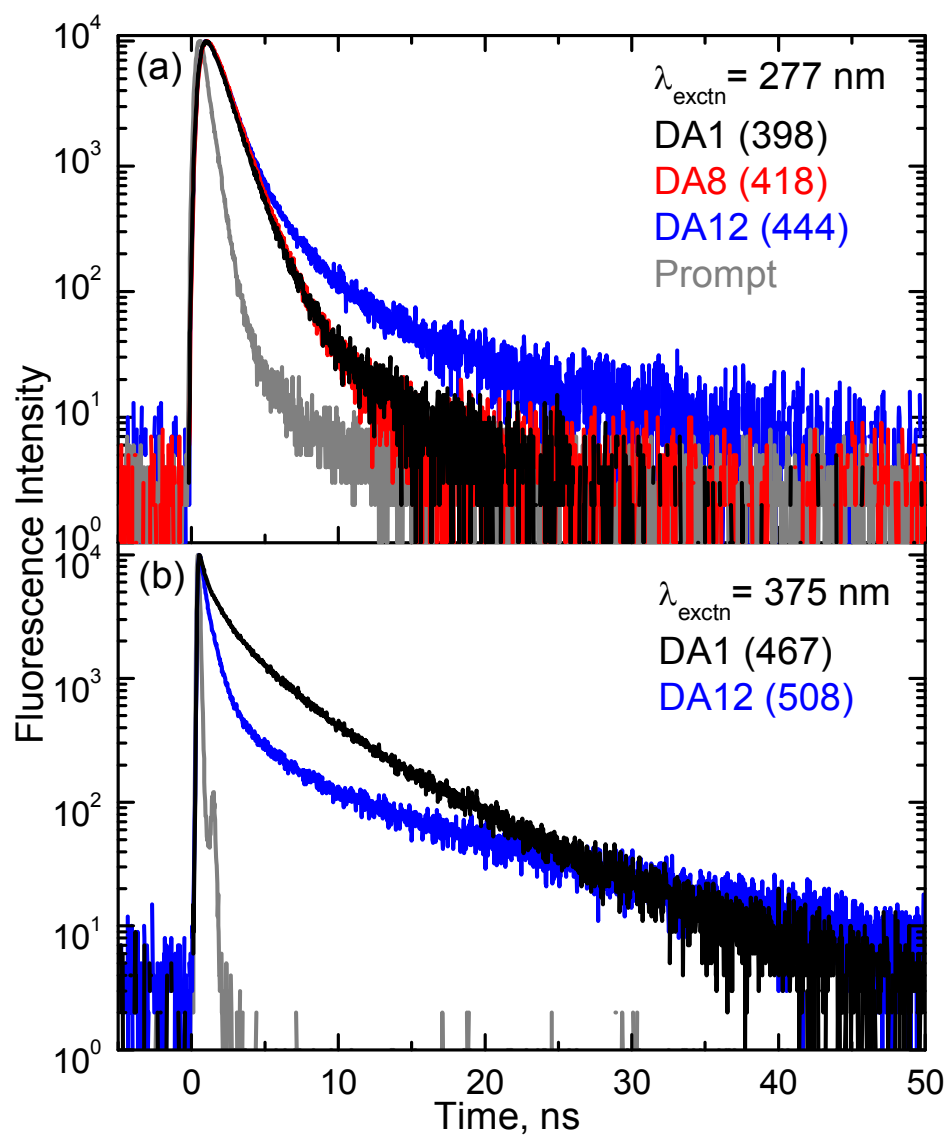


**Figure 9** Solid state fluorescence decay profiles of DA derivatives obtained by exciting at 277 (a) and 375 nm (b). The materials of DA1, DA8 and DA12 are given black, red and blue respectively. The probing wavelength in nm is given in the bracket.

For the **DA8** and **DA12**, the lifetimes of 0.84 and 1.06 ns were obtained respectively by exciting at 277 nm and probing at 418 and 444 nm respectively. In the case of **DA12** materials, when probed at 508 nm by exciting at 375 nm long lived lifetime of 6.3 ns is obtained. Similarly fluorescence lifetime of 0.81, 0.71 and 0.70 ns were obtained for **MA1**, **MA8** and **MA12** materials by exciting at 277 nm and probing at their emission maxima. The lifetime components of ~0.7–0.81 ns could be due to the monomer emission of the materials. Whereas long lived components of 6.88 (**MA8**) and 7.15 (**MA12**) ns were obtained by exciting at 375 nm and probing at 418 nm.

In both the **MA** and **DA** derivatives long lived components were observed on exciting at the red side of the absorption spectra and probing at red side of monomer emission spectra suggesting that they could be attributed to J-type aggregates. J-aggregates are however characterized by very short life-times (high radiative constants). The unusually long lived emission could arise from the rearrangement of the J-aggregates in the excited state to some form of excimers as suggested earlier for some other molecular systems<sup>35, 42</sup>.

### 3.3 Photophysical Properties of DA1 Crystals

The single crystals (**DA1C**) were obtained for the **DA1** materials by slow crystallization using small amount of materials dissolved in THF. The absorption and emission spectra of **DA1C** are shown in Figure 10. The absorption spectra of **DA1C** showed broad maximum around ~310 and 370 nm as in the powder form of **DA1**. In Figure 10, when excitation wavelength was changed from 300 to 360 nm, there was an increase of emission intensity at around 396 nm. With further increase of excitation wavelength to 400 nm a decrease of intensity around 396 nm were observed. The excitation spectra of **DA1C** are given in the Supporting Information (Figure S9). The fluorescence lifetime of **DA1C** were measured by exciting at 277 nm and probing at 396 nm. The major lifetime component of

0.85 ns was obtained, which was similar to the monomer emission time constant of **DA1**. This reflects that crystals consist of purely monomeric form of **DA1** and consistent with the single crystal X-ray structure which is given below.

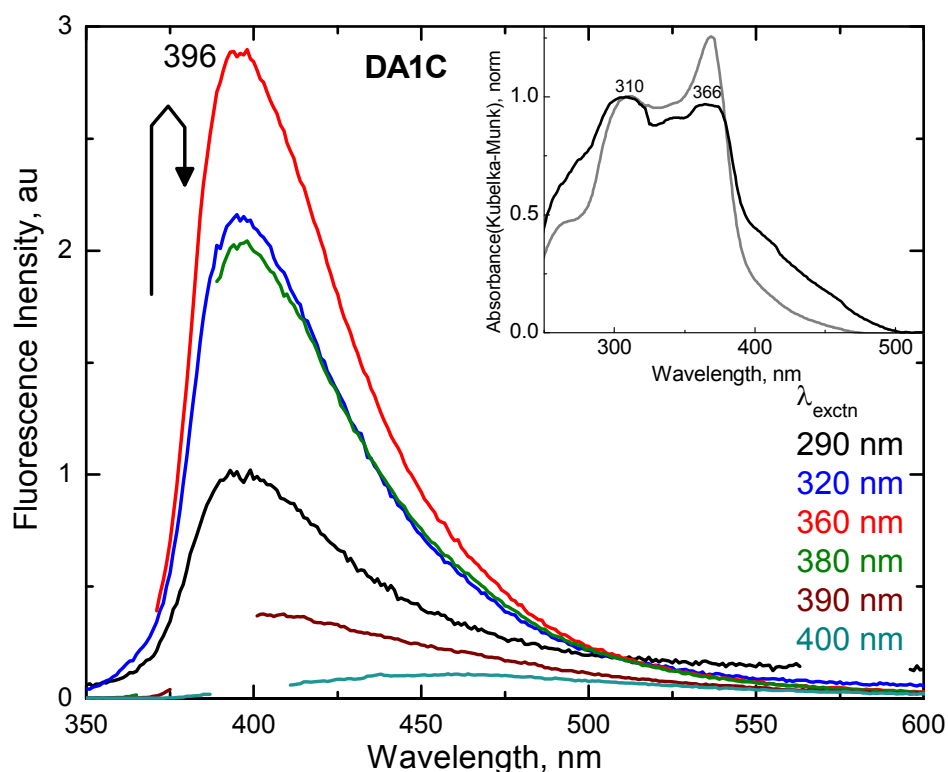


**Figure 10** Solid state absorption (insets) and fluorescence spectra of **DA1C**. The solid state absorption spectra of **DA1** is also given in grey colour for comparison (insets). The representative excitation wavelengths are given in different colours. The spectral changes with increase of excitation wavelength are shown by the arrow.

In order to characterize the presence of different fluorescence components in the **DA1** materials, the time resolved emission spectra of different polymorphic forms viz., crystal (**DA1C**) and powder (**DA1**) were measured. Figure 11a shows the time resolved emission spectra of **DA1** recorded at a time scale starting from 0.6 to 2.3 ns by exciting at 277 nm. At short time, the spectra showed emission maximum around 410 nm with broad shoulder around 540 nm. With increase of time, the overall spectral intensity decreases. Whereas **DA1C** showed only a maximum of around 400 nm without broad shoulder around 540 nm for the similar spectral time (Figure 11b). These observations are similar with the steady state emission spectra of the respective materials (Figure 7a and 10). The time resolved emission spectra of **DA1** shows a peak around 460 nm at longer spectral time by exciting at 375 nm (Figure S10) and time constant found to be 12.5 ns as mentioned earlier.

The single crystal data of **DA1C** is summarized in Table 5. Figure 12a and b show the unit cell and molecular arrangement down the *b* axis respectively. Figure 12c and d represent the two major alignments of the molecules in the crystal. The crystal structure consists of four monomer molecules per unit cell and the **DA1** molecules are arranged in a co-facial manner with dipole moments of neighbouring stacks oriented in opposite directions. Nevertheless the molecules have an offset packing along the short molecular axis leading to a minimized  $\pi$ -overlap. The dihedral angle between benzonitrile and dimethoxy benzene groups is 27.22°. The two methoxy groups are in planar with the benzene. In the stacking direction, the down the *a*-axis the major stabilizing forces are  $\pi$ - $\pi$  (average distance of 3.96 Å) and C-H- $\pi$  interaction (3.2Å). In addition along *c*-axis molecular stacks make C-H...O as well as C-H...N hydrogen bonding interaction. The details of the interaction are provided in the Table S6. Unique molecule of **DA1** interacts with three adjacent molecules through OCH<sub>3</sub> moieties.

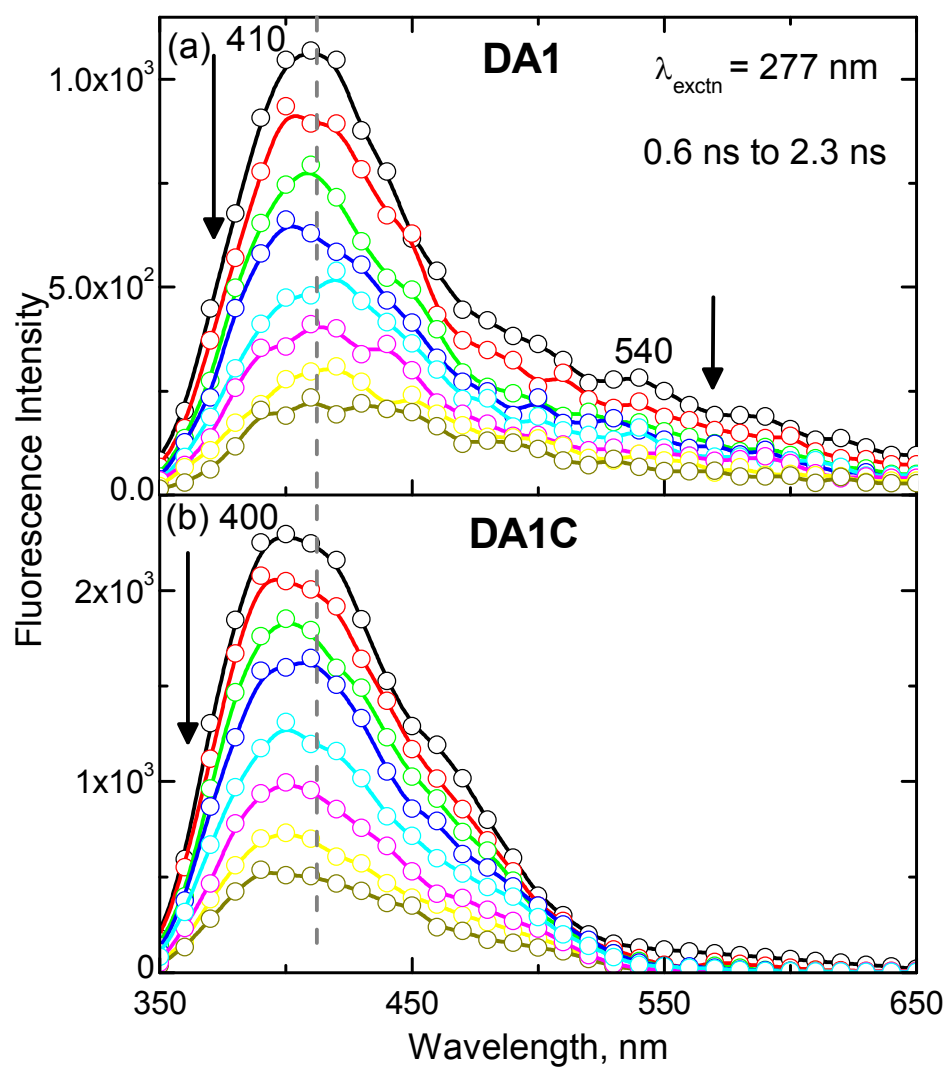


**Figure 11** (a) Time-resolved emission spectra of DA1(a) and DA1C (b) materials recorded from 0.6 to 2.3 ns by exciting at 277 nm.

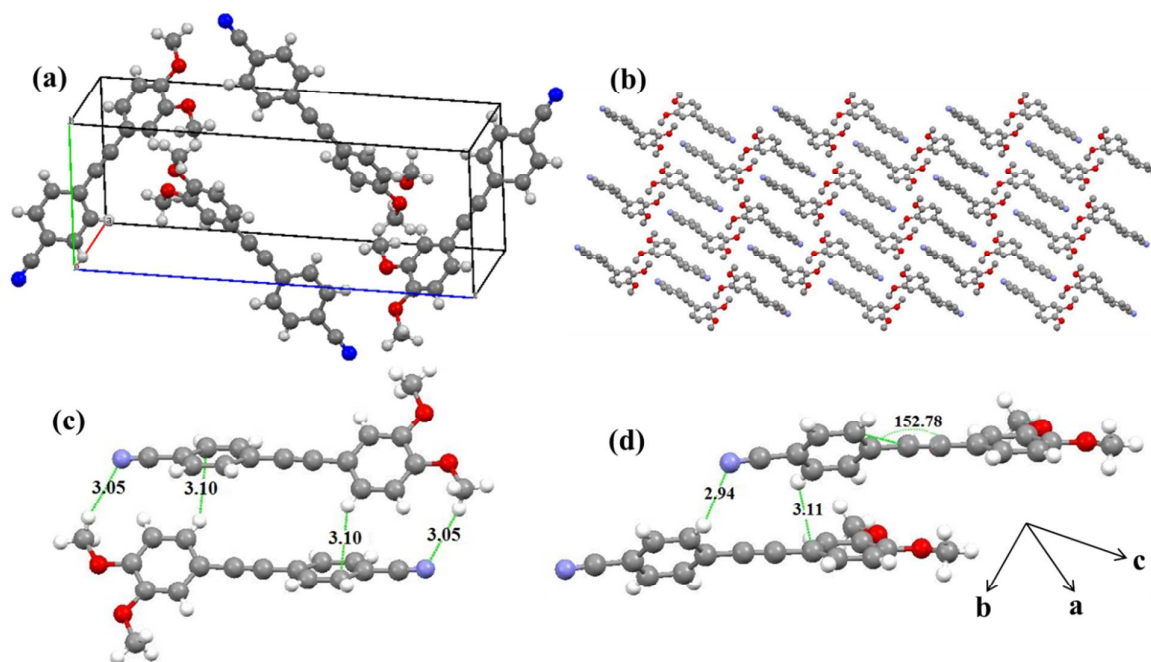


**Figure 12** (a) Crystal structure of **DA1** showing a unit cell, (b) molecular packing. (c) and (d) dimer units showing the interactions.

Thus the crystal structure consists of four monomer molecules and stabilized through a network of weak interactions and the  $\pi$ -stacked columns are held together by weak C–H $\cdots$ N and C–H $\cdots$ O interactions.

Powder XRD measurements were carried out for all the materials and are shown in Supporting Information as Figure S11. From the diffraction pattern, it is clear that all are in crystalline form. The XRD diffraction pattern of powder and crushed crystals of **DA1** are shown in Supporting Information as Figure S12 for comparison. The rich diffractive pattern reflects the highly crystalline nature of these materials. When compared to **DA1C**, there were few new peaks observed at 7.57 (11.7Å), 9.33 (9.5Å) and 11.00 (8.06Å) in **DA1** reflecting weak phase mixing due to the difference in molecular packing in the two materials.

## 5. Summary

In summary, push-pull chromophores of cyano and mono/bisalkoxy substituted diphenylacetylene derivatives were synthesized and their solvatochromic and polymorphic behaviours were characterized. In solution red shifted fluorescence, increase of fluorescence quantum yields and their lifetimes were obtained in the bis alkoxy derivatives when compared to mono alkoxy derivatives. This could be attributed to increasing electron donating ability of additional alkoxy group causing the increased formation of the fluorescent intramolecular charge transfer state. It is interesting to note that the emission quantum yields of these materials in solid state were significantly higher than in solution. The **DA1** derivative exhibited interesting polymorphic behaviour where powder form showed significantly different photophysical properties when compared to crystalline form (**DA1C**). The difference is attributed to the presence of different fluorescence component including monomer, J- and H-type aggregates in the powder form. Whereas in the crystalline form the fluorescence arise from the monomer and consistent with the single crystal X- ray structure.

### ASSOCIATED CONTENT

#### Supporting information

Detailed synthetic procedures and characterization of compounds are given. The absorption, emission and excitation spectra of **DA1** in acetonitrile and cyclohexane (Figure S1), the absorption and emission spectra of **MA1**, **MA8** and **MA12** in different solvents (Figure S2), fluorescence decay profiles of **DA** and **MA** derivatives in solution (Figure S3), absorption spectra of **DA1** in decane with increase of concentration (Figure S4), normalized solid state fluorescence spectra of **DA** derivatives (Figure S5), solid state excitation spectra of **DA1** (Figure S6), absorption, emission and excitation spectra of **DA1** in KBr (0.002%) (Figure S7), solid state fluorescence decay profiles of **MA** derivatives (Figure S8), excitation

spectra of **DA1C** (Figure S9), time resolved emission spectra of **DA1** obtained by 375 nm excitation (Figure S10), powder XRD spectra of all the derivatives (Figure S11 and 12), key optimized structures and theoretical data of **DA1** and **MA1** by CAM B3LYP/6-31G(d), the spectroscopic and photophysical data of **MA8** (Table S1), **DA8** (Table S2), **MA12** (Table S3), **DA12** (Table S4) and details of crystal data **DA1C** (Table S5) are provided.

## AUTHOR INFORMATION

### Corresponding Author

\*Fax: (+91) 471-2490186. E-mail: [k.venugopal@niist.res.in](mailto:k.venugopal@niist.res.in) and [sureshdas@niist.res.in](mailto:sureshdas@niist.res.in)

### Notes

The authors declare no competing financial interest.

## ACKNOWLEDGMENT

K.V gratefully acknowledges DST-SERB, Government of India for financial support. This work is supported by Council of Scientific and Industrial Research (CSIR) under the Project NWP 55. D. P. thanks CSIR for research fellowships. The authors thank Lighi Das and Archana A. for helping in synthesis and preliminary studies. The authors thank also Dr. C. H. Suresh and Dr. V. Prabha for allowing to do theoretical calculation using computational facility and fruitful discussion.

## References

1. Y. Tao, K. Yuan, T. Chen, P. Xu, H. Li, R. Chen, C. Zheng, L. Zhang and W. Huang, *Adv Mater*, 2014, **26**, 7931-7958.
2. H. Nakanotani, T. Higuchi, T. Furukawa, K. Masui, K. Morimoto, M. Numata, H. Tanaka, Y. Sagara, T. Yasuda and C. Adachi, *Nat. Commun.*, 2014, **5**.

3. R. D. Costa, E. Ortí, H. J. Bolink, F. Monti, G. Accorsi and N. Armaroli, *Angew.Chem.Int. Ed.*, 2012, **51**, 8178-8211.
4. B. W. D'Andrade and S. R. Forrest, *Adv Mater*, 2004, **16**, 1585-1595.
5. Z.-K. Tan, R. S. Moghaddam, M. L. Lai, P. Docampo, R. Higler, F. Deschler, M. Price, A. Sadhanala, L. M. Pazos, D. Credgington, F. Hanusch, T. Bein, H. J. Snaith and R. H. Friend, *Nat. Nano.*, 2014, **9**, 687-692.
6. J. W. Rumer, S.-Y. Dai, M. Levick, Y. Kim, M.-B. Madec, R. S. Ashraf, Z. Huang, S. Rossbauer, B. Schroeder, L. Biniek, S. E. Watkins, T. D. Anthopoulos, R. A. J. Janssen, J. R. Durrant, D. J. Procter and I. McCulloch, *J. Mater.Chem.C*, 2013, **1**, 2711-2716.
7. S. Reineke, F. Lindner, G. Schwartz, N. Seidler, K. Walzer, B. Lussem and K. Leo, *Nature*, 2009, **459**, 234-238.
8. S. Kena Cohen and S. R. Forrest, *Nat. Photon.*, 2010, **4**, 371-375.
9. V. M. Agranovich, Y. N. Gartstein and M. Litinskaya, *Chem. Rev.*, 2011, **111**, 5179-5214.
10. M. Muccini, *Nat. Mater.*, 2006, **5**, 605-613.
11. H. T. Yi, M. M. Payne, J. E. Anthony and V. Podzorov, *Nat. Commun.*, 2012, **3**, 1259.
12. Y. Yamaguchi, K. Ogawa, K.-i. Nakayama, Y. Ohba and H. Katagiri, *J. Am. Chem. Soc.*, 2013, **135**, 19095-19098.
13. C. Kanimozhi, N. Yaacobi-Gross, K. W. Chou, A. Amassian, T. D. Anthopoulos and S. Patil, *J. Am. Chem. Soc.*, 2012, **134**, 16532-16535.
14. M. Gsänger, E. Kirchner, M. Stolte, C. Burschka, V. Stepanenko, J. Pflaum and F. Würthner, *J. Am. Chem. Soc.*, 2014, **136**, 2351-2362.
15. D. Ding, K. Li, B. Liu and B. Z. Tang, *Acc. Chem. Res.*, 2013, **46**, 2441-2453.

16. K. E. Achyuthan, T. S. Bergstedt, L. Chen, R. M. Jones, S. Kumaraswamy, S. A. Kushon, K. D. Ley, L. Lu, D. McBranch, H. Mukundan, F. Rininsland, X. Shi, W. Xia and D. G. Whitten, *J. Mat. Chem.*, 2005, **15**, 2648-2656.
17. S. Varghese and S. Das, *J. Phys. Chem. Lett.*, 2011, **2**, 863-873.
18. A. Zitzler-Kunkel, M. R. Lenze, T. Schnier, K. Meerholz and F. Würthner, *Adv Funct Mater*, 2014, **24**, 4645-4653.
19. J. B. Birks, *Photophysics of Aromatic Molecules*, Wiley, London, 1970.
20. J. Malkin, *Photophysical and Photochemical Properties of Aromatic Compounds*, CRC, Boca Raton, 1992.
21. N. J. Turro, *Modern Molecular Photochemistry*, University Science Books, Mill Valley, 1991.
22. Y. Hong, J. W. Y. Lam and B. Z. Tang, *Chem. Soc. Rev.*, 2011, **40**, 5361-5388.
23. B.-K. An, J. Gierschner and S. Y. Park, *Acc. Chem. Res.*, 2011, **45**, 544-554.
24. Y. Hong, J. W. Y. Lam and B. Z. Tang, *Chem. Commun.*, 2009, 4332-4353.
25. G. Scheibe, *Angew. Chem.*, 1937, **50**, 212-219.
26. E. E. Jelley, *Nature*, 1936, **138**.
27. F. Würthner, T. E. Kaiser and C. R. Saha-Möller, *Angew. Chem. Int. Ed.*, 2011, **50**, 3376-3410.
28. V. Czikkely, H. D. Forsterling and H. Kuhn, *Chem. Phys. Lett.*, 1970, **6**, 207-210.
29. F. Nüesch and M. Grätzel, *Chem. Phys.*, 1995, **193**, 1-17.
30. A. Qin, C. K. W. Jim, Y. Tang, J. W. Y. Lam, J. Liu, F. Mahtab, P. Gao and B. Z. Tang, *J. Phys. Chem. B*, 2008, **112**, 9281-9288.
31. U. Rösch, S. Yao, R. Wortmann and F. Würthner, *Angew. Chem. Int. Ed.*, 2006, **45**, 7026-7030.
32. S. Zeena and K. G. Thomas, *J. Am. Chem. Soc.*, 2001, **123**, 7859-7865.

33. Z. Chen, V. Stepanenko, V. Dehm, P. Prins, L. D. A. Siebbeles, J. Seibt, P. Marquetand, V. Engel and F. Würthner, *Chem. Eur.J.*, 2007, **13**, 436-449.
34. J. M. Lim, P. Kim, M.-C. Yoon, J. Sung, V. Dehm, Z. Chen, F. Wurthner and D. Kim, *Chem. Sci.*, 2013, **4**, 388-397.
35. S. A. Z. Jenekhe, X.; Yi, S., *Technical report no.5, Office of Naval Research*, 1999.
36. S. Priyadarshy, M. J. Therien and D. N. Beratan, *J.Am.Chem.Soc.*, 1996, **118**, 1504-1510.
37. D. Holten, D. F. Bocian and J. S. Lindsey, *Acc. Chem. Res.*, 2002, **35**, 57-69.
38. Y. Hirata, T. Okada and T. Nomoto, *J.Phys.Chem.*, 1993, **97**, 9677-9681.
39. C. Ferrante, U. Kensy and B. Dick, *J. Phys. Chem.*, 1993, **97**, 13457-13463.
40. T.-a. Ishibashi and H.-o. Hamaguchi, *J. Phys. Chem. A*, 1998, **102**, 2263-2269.
41. N. Tamai, T. Nomoto, F. Tanaka, Y. Hirata and T. Okada, *J. Phys.Chem. A*, 2002, **106**, 2164-2172.
42. V. Karunakaran, D. D. Prabhu and S. Das, *J. Phys. Chem. C*, 2013, **117**, 9404-9415.
43. R. Thomas, S. Lakshmi, S. K. Pati and G. U. Kulkarni, *J. Phys. Chem. B*, 2006, **110**, 24674-24677.
44. W. L. F. Amarego and L. L. C. Chai, *Purification of Laboratory Chemicals*, Fifth Edition edn., Elsevier Science, Burlington, MA, 2003.
45. L. O. Palsson and A. P. Monkman, *Adv Mater*, 2002, **14**, 757-758.
46. M. Colle, J. Gmeiner, W. Milius, H. Hillebrecht and W. Brutting, *Adv Funct Mater*, 2003, **13**, 108-112.
47. CrystalClear2.1, *Rigaku Corporation*, Tokyo, Japan.
48. J. W. Pflugrath, *Acta Crystallogr. Sect. D*, 1999, **55**, 1718-1725.
49. G. M. Sheldrick, University of Gottingen, 1996.
50. A. L. Spek, University of Utrecht, 1995.

51. M. J. Frisch, G. W. Trucks, H. B. Schlegel, G. E. Scuseria, M. A. Robb, J. R. Cheeseman, G. Scalmani, V. Barone, B. Mennucci, G. A. Petersson, H. Nakatsuji, M. Caricato, X. Li, H. P. Hratchian, A. F. Izmaylov, J. Bloino, G. Zheng, J. L. Sonnenberg, M. Hada, M. Ehara, K. Toyota, R. Fukuda, J. Hasegawa, M. Ishida, T. Nakajima, Y. Honda, O. Kitao, H. Nakai, T. Vreven, J. A. Montgomery, J. E. Peralta, F. Ogliaro, M. Bearpark, J. J. Heyd, E. Brothers, K. N. Kudin, V. N. Staroverov, R. Kobayashi, J. Normand, K. Raghavachari, A. Rendell, J. C. Burant, S. S. Iyengar, J. Tomasi, M. Cossi, N. Rega, J. M. Millam, M. Klene, J. E. Knox, J. B. Cross, V. Bakken, C. Adamo, J. Jaramillo, R. Gomperts, R. E. Stratmann, O. Yazyev, A. J. Austin, R. Cammi, C. Pomelli, J. W. Ochterski, R. L. Martin, K. Morokuma, V. G. Zakrzewski, G. A. Voth, P. Salvador, J. J. Dannenberg, S. Dapprich, A. D. Daniels, Farkas, J. B. Foresman, J. V. Ortiz, J. Cioslowski and D. J. Fox, Wallingford CT, 2009.
52. A. Demeter, S. Druzhinin, M. George, E. Haselbach, J.-L. Roulin and K. A. Zachariasse, *Chem. Phys. Lett.*, 2000, **323**, 351-360.
53. W. Rettig, *In Topics of Current Chemistry; Electron Transfer*, Springer, Berlin, 1994.
54. N. S. S. Kumar, S. Varghese, N. P. Rath and S. Das, *J. Phys. Chem. C*, 2008, **112**, 8429-8437.
55. R. Davis, N. S. Saleesh Kumar, S. Abraham, C. H. Suresh, N. P. Rath, N. Tamaoki and S. Das, *J. Phys. Chem. C*, 2008, **112**, 2137-2146.
56. P. R. Bangal, S. Panja and S. Chakravorti, *J. Photochem. Photobiol. A: Chem.*, 2001, **139**, 5-16.
57. N. Mataga, Y. Kaifu and M. Koizumi, *Bull. Chem. Soc. Jpn.*, 1956, **29**, 465-470.
58. J. R. Lakowicz, *Principles of Fluorescence Spectroscopy*, Springer, New York, 2006.

59. M. Khajepour and J. F. Kauffman, *J. Phys. Chem. A*, 2001, **105**, 10316-10321.
60. F. Fennel, S. Wolter, Z. Xie, P.-A. Plötz, O. Kühn, F. Würthner and S. Lochbrunner, *J. Am. Chem. Soc.*, 2013, **135**, 18722-18725.
61. J. Gierschner and S. Y. Park, *J. Mat. Chem. C*, 2013, **1**, 5818-5832.
62. A. B. Koren, M. D. Curtis and J. W. Kampf, *Chem. Mater.*, 2000, **12**, 1519-1522.
63. Z. Xie, B. Yang, F. Li, G. Cheng, L. Liu, G. Yang, H. Xu, L. Ye, M. Hanif, S. Liu, D. Ma and Y. Ma, *J. Am. Chem. Soc.*, 2005, **127**, 14152-14153.
64. H. Sun, Z. Zhao, F. C. Spano, D. Beljonne, J. Cornil, Z. Shuai and J. L. Brédas, *Adv Mater*, 2003, **15**, 818-822.

**Table 1** Absorption and fluorescence maxima, quantum yields, lifetime, radiative and non-radiative rate constants of **DA1** in various solvents

Solvents	Dielectric constant, $\epsilon$	Refractive index, $n$	Absorption max ( $\lambda_{\max}$ ), nm	Fluorescence max ( $\lambda_{\max}$ ), nm	Stokes shift ( $\Delta\nu$ ), $\text{cm}^{-1}$	Fluorescence quantum yield, $\Phi_f$	Fluorescence lifetime ( $\tau$ ), ns	Radiative constant ( $K_r$ ), $10^9 \text{ s}^{-1}$	Non radiative constant ( $K_{nr}$ ), $10^9 \text{ s}^{-1}$
n-hexane	1.88	1.3723	322, 343	346	253	0.16	0.37	0.42	2.31
n-heptane	1.92	1.3851	322, 344	347	251	0.16	0.38	0.41	2.22
1,4-dioxane	2.21	1.4203	326	400	5,675	0.16	1.09	0.14	0.77
Chloroform	4.89	1.442	329	404	5,643	0.18	0.89	0.20	0.93
Ethyl acetate	6.02	1.3698	326	408	6,165	0.13	1.00	0.13	0.87
Dichloromethane	9.08	1.4242	331	417	6,231	0.22	1.25	0.17	0.63
1-propanol	20.1	1.387	329	425	6,866	0.13	0.95	0.14	0.91
Acetonitrile	35.94	1.341	325	451	8,596	0.13	2.03	0.07	0.43
Dimethyl sulphoxide	46.45	1.477	334	462	8,295	0.21	2.51	0.08	0.32

Fluorescence lifetimes were obtained by exciting at 335 nm and  $\chi^2$  value of fluorescence kinetics fit is between 1.0 to 1.2.

**Table 2** Absorption and fluorescence maxima, quantum yields, lifetime, radiative and non-radiative rate constants of MA1 in various solvents

Solvents	Dielectric constant, $\epsilon$	Refractive index, $n$	Absorption max ( $\lambda_{\text{max}}$ ), nm	Fluorescence max ( $\lambda_{\text{max}}$ ), nm	Stokes shift ( $\Delta\nu$ ), $\text{cm}^{-1}$	Fluorescence quantum yield, $\Phi_f$	Fluorescence lifetime, ( $\tau$ ), ns	Radiative constant, ( $K_r$ ), $10^9 \text{ s}^{-1}$	Nonradiative constant, ( $K_{nr}$ ), $10^9 \text{ s}^{-1}$
n-hexane	1.88	1.3723	310, 331	336	450	0.15	0.34	0.45	2.47
n-heptane	1.92	1.3851	311, 332	337	447	0.17	0.35	0.49	2.36
1,4-dioxane	2.21	1.4203	315, 330	369	3,203	0.10	0.33	0.31	2.72
Chloroform	4.89	1.442	319, 332	374	3,383	0.13	0.38	0.35	2.28
Ethyl acetate	6.02	1.3698	314, 328	377	3,963	0.08	0.38	0.22	2.41
Dichloromethane	9.08	1.4242	319, 330	386	4,396	0.12	0.46	0.26	1.91
1-propanol	20.1	1.387	317, 328	395	5,171	0.13	0.60	0.22	1.45
Acetonitrile	35.94	1.341	314, 324	411	6,533	0.09	0.76	0.12	1.20
Dimethyl sulphoxide	46.45	1.477	319, 329	418	6,472	0.15	1.10	0.14	0.76

Fluorescence lifetimes were obtained by exciting at 335 nm and  $\chi^2$  value of fluorescence kinetics fit is between 1.0 to 1.2.

**Table 3** Results of CAM B3LYP/6-31G(d) calculations for all the derivatives

Compound	Energy, eV	$\lambda_{\max}$ , nm <sup>a</sup>	$f_{os}$ <sup>b</sup>	Main Transitions (weight) <sup>c</sup>	$\mu_g$ , Debye
<b>DA1</b>	3.66	312.8	1.22	H→L (100%)	6.72
		183.9	0.78	H-1 → L (100%)	
<b>DA8</b>	3.71	311.8	1.32	H→L (100%)	9.36
		180.6	0.56	H-1 → L (100%)	
<b>DA12</b>	3.72	311.4	1.33	H→L (100%)	7.57
		181.1	0.62	H-1 → L (100%)	
<b>MA1</b>	3.85	305.8	1.26	H→L (100%)	6.87
		177.8	1.22	H-1 → L (100%)	
<b>MA8</b>	3.83	307.1	1.37	H→L (100%)	8.00
		178.0	1.35	H-1 → L (55%); H→L+3 (45%)	
<b>MA12</b>	3.83	307.2	1.38	H→L (100%)	8.05
		178.0	1.36	H-1 → L (55%); H→L+3 (45%)	

<sup>a</sup> $\lambda_{\max}$  value obtained from the simulated absorption spectrum, <sup>b</sup> only transitions with  $f_{os} > 0.5$  are included <sup>c</sup>H= HOMO, L= LUMO

**Table 4** Solid state absorption and emission maxima, emission lifetimes and quantum yields for all the derivatives<sup>a</sup>

Compounds	$\lambda_{\text{abs}}$ nm	$\lambda_{\text{flu}}$ nm	$\lambda_{\text{exctn}}/\lambda_{\text{probe}}$ nm	$\tau_1$ ns	$A_1$ %	$\tau_2$ ns	$A_2$ %	$\tau_3$ ns	$A_3$ %	$\chi^2$	$\Phi$	$K_r$ , $10^9 \text{ s}^{-1}$	$K_{nr}$ , $10^9 \text{ s}^{-1}$
<b>DA1</b>	310, 370	398,467, 543	277 / 398	<u>0.93 ± 0.03</u>	86.81	2.3 ± 0.08	13.19			1.07	0.79 ± 0.04	0.014	0.89
			277/ 543	<u>1.31 ± 0.05</u>	75.55	8.7 ± 0.10	24.45			1.14			
			375 / 467	0.48 ± 0.02	10.55	1.10 ± 0.05	13.28	<u>12.31 ± 0.20</u>	76.17	1.29			
<b>DA1C</b>	310,370	396	277 / 396	<u>0.85 ± 0.03</u>	95.45	5.93 ± 0.08	4.55			1.20	0.54 ± 0.03	0.020	0.90
<b>DA8</b>	310, 370	418	277 / 418	<u>0.84 ± 0.04</u>	76.13	1.61 ± 0.05	23.87			1.07	0.13 ± 0.02	0.079	0.90
<b>DA12</b>	310, 370	444, 422 <sup>s</sup>	277 / 444	0.33± 0.02	24.66	<u>1.06 ± 0.04</u>	<u>67.96</u>	6.51 ± 0.10	7.39	1.10	0.32 ± 0.02	0.039	0.74
			375 / 530	0.30± 0.02	10.73	1.83 ± 0.03	41.02	<u>6.36 ± 0.10</u>	48.25	1.30			
<b>MA1</b>	362, 310 <sup>s</sup>	391, 409 <sup>s</sup>	277/ 391	<u>0.81± 0.03</u>	64.71	2.7 ± 0.06	35.29			1.11	0.65 ± 0.02	0.023	0.65
<b>MA8</b>	320	366	277 / 366	<u>0.71± 0.02</u>	95.97	4.30 ± 0.10	4.03			1.19	0.54 ± 0.03	0.016	1.15
			375 / 418	0.37± 0.01	29.66	1.81 ± 0.05	28.58	<u>6.88 ± 0.10</u>	41.76	1.12			
<b>MA12</b>	304	366, 409 <sup>s</sup>	277 / 366	<u>0.70± 0.02</u>	92.24	4.52 ± 0.10	7.76				0.60 ± 0.03	0.017	0.99
			375 / 418	<u>0.39± 0.02</u>	14.61	2.00 ± 0.05	40.93	<u>7.15 ± 0.11</u>	44.46	1.30			

<sup>a</sup>  $\lambda_{\text{abs}}$ —absorption maximum,  $\lambda_{\text{flu}}$ —fluorescence maximum,  $\lambda_{\text{exctn}}/\lambda_{\text{probe}}$ —excitation and probing wavelength,  $\tau$ —lifetime,  $A$ —amplitude,  $\Phi$ —quantum yield,  $K_r$ —radiative constant,  $K_{nr}$ —non radiative constant, s—shoulder, and major components are underlined.

**Table 5** Summary of crystallographic data for **DA1**<sup>a</sup>

<b>DA1</b>	
Empirical formula	C <sub>17</sub> H <sub>13</sub> NO <sub>2</sub>
Molecular weight	263.28
Crystal system	Monoclinic
Space group	P 21/n
Z	4
a, Å	8.804 (7)
b, Å	7.685 (5)
c, Å	21.631(15)
α, deg	90.00
β, deg	100.287(12)
γ, deg	90.00
V, Å <sup>3</sup>	1439.9(18)
d <sub>cal</sub> , Mg/cm <sup>3</sup>	1.214
μ, mm <sup>-1</sup>	0.077
Total reflection	11239
Unique reflection	2973
R <sub>int</sub>	0.0755
Final R indices (wR2)	0.1936

<sup>a</sup>Cambridge crystal data center (CCDC 1050424).

## Table of Contents Image (TOC)

The variation of photophysical properties of cyano and alkoxy substituted diphenylacetylene derivatives from solution to solid state revealed the important role of self-aggregation on these properties.

